On the Ideal Diamagnetism of Composite Graphene and Graphite Nanostructures

A. Rzhevskii[1], S. Chahid[2], R. Dulal[2], S. Teknowijoyo[2] and A. Gulian[2,*]

[1] Thermo Fisher Scientific, 2 Radcliff Rd., Tewksburry, MA 01876, USA
[2] Advanced Physics Laboratory, Chapman University, Burtonsville, MD 20866, USA
* gulian@chapman.edu

ABSTRACT

Graphite and its derivatives such as graphene have demonstrated many unique properties that are still under intense exploration. In particular, these properties are important for microelectronics applications. In our case it was ideal diamagnetism in composite graphene system where the reproducibility on demand suffered. The quality of graphene and influence of humidity were recognized as possible cause of this problem. Thus, we performed systematic studies of the quality of pristine graphene and its degradation vs. various conditions. Raman studies constituted an essential part of research and are reported in detail. Specimens on different substrates were explored via application of annealing (at $100°C - 480°C$, in air and in a vacuum) to vary physical properties of graphene. We complemented Raman mapping by characterizing the morphology of films using AFM scans.

Keywords: ideal diamagnetism, composite structure, graphene, permalloy, n-heptane

1 INTRODUCTION

Graphene is a classic $2D$ material, a single layer of sp^2 bonded carbon atoms arranged in a hexagonal lattice. Different methods were used to synthesize graphene, among them, Hummer's method, chemical exfoliation, epitaxial growth and chemical vapor deposition, CVD (see reviews [1]-[6] for various mentioned methods). Due to its exotic physical properties, graphene is being used in many electronics applications [2]-[4]. For these applications, it should be transferred from its original growth location, typically transition metal surface (at most widely used CVD deposition), such as copper or nickel foil, to a dielectric solid substrate, such as Si/SiO_2 [7, 8]. This transferring procedure consists of covering the graphene layer by a plastic material, such as poly(methyl methacrylate) $PMMA$, then removal of the copper substrate by an etchant, such as iron dichloride. The etchant residues are washed away by immersing into deionized water. Finally, the plastic film with graphene is placed on the solid substrate, and subsequently dissolved by, say, acetone [8, 9]. However, cracks, gaps and low adhesion between graphene and substrates are the main defects

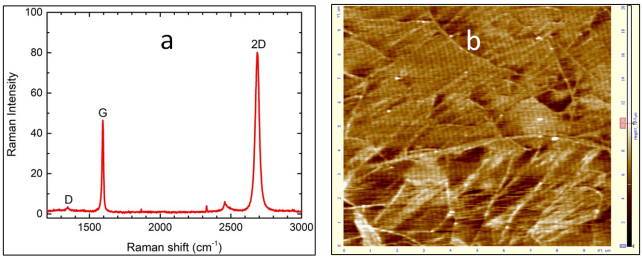

Figure 1: (a) Typical Raman spectrum of single layer graphene has its $G-$peak twice shorter than $2D-$peak. The $D-$peak is vanishing when the impurities are absent. When two or more layers are present, the relative height ratio $G/2D$ becomes larger. Impurities would increase the height of the $D-$peak. (b) AFM pattern of the same sample has wrinkles (thin white lines) and domain-type regions caused most likely by the granular structure of copper support at initial growing by CVD process. Both wrinkles and larger size "domains" remain after the transfer.

observed using this method [10]-[12]. The copper foil surface is not ideally smooth at the growth/deposition of graphene. As a consequence, the transferred graphene does not lie down flat on the top of the target substrate. To improve the flatness and residue problems , the second layer of $PMMA$ is deposited after the graphene transfer to the target substrate [6, 10, 13]. Unfortunately, even without this second layer, the acetone rinsing after transfer leaves a thin layer of $PMMA$ on the graphene surface which leads to the altered properties [7, 12, 14, 15]. Thus, its surface should be functionalized for unrestricted electron passage to electrodes, interaction with dopants and interfaces, etc. [11],[16]-[22]. Manufacturers typically test the results by Raman analysis [23], and good quality single layer graphene should have signals like in Fig.1,a.

However, even for these "good" samples the quality may be not high enough, as Fig. 1b demonstrates. We encountered these obstacles when performing experiments with graphene-permalloy-alkane condensed matter research [24] - sometimes, samples tested as very good by Raman mapping were not revealing the features which other samples did. These features include ideal diamagnetic type response by the structure graphene-

permalloy at the addition of n-heptane. The details are described in [24]. Previous studies have demonstrated that the physical properties of graphene can be altered in graphene-liquid systems [25]-[32]. Our initial goal was to observe diamagnetism in the graphene-$n-$heptane system. This effect is an important observation, since it takes place at room temperatures, and until now, the ideal diamagnetism is a property of only one quantum object: the superconductor. That is why the reproducibility of diamagnetism requires an understanding of circumstances which prohibit it.

In addition to sporadic absence of diamagnetism at the $n-$heptane injection, typically, reuse of successfully signal-developed graphene is not possible. That was an additional reason for aposteriori studies of the used graphene samples. A special test procedure was used which involved Raman and AFM studies of graphene samples before and after soaking them into $n-$heptane. The results are described in this article.

2 MATERIALS AND METHODS

2.1 Graphene Samples

We used in experiments mainly single layer graphene on Si/SiO_2 substrates manufactured by Cheap Tubes Inc. (USA) and Graphene Platform (Japan). Typical treatments by $n-$heptane were made in two different ways: 1) drop of $n-$heptane onto the graphene surface, wait for evaporation (about 1 h) and the Raman and AFM studies; 2) soaking the graphene sample into $n-$heptane using a glass bicker for about 1 h, drying in air at ambient temperature for many hours, and then the above mentioned studies.

2.2 Raman Spectroscopy

The Raman spectra are taken at ambient temperature using a Thermo Fisher DXR Raman microscope equipped with a 532 nm (green) unpolarized excitation laser and a 5 cm^{-1} resolution grating. The calibration is performed automatically using an internally attached calibration toolkit which includes a standard polystyrene film. Using a $10\times$ objective and a 50 micron pinhole, the estimated laser spot size at the sample is ~ 2 micron. The laser power is kept at 3 mW, and the total exposure time is 2 minutes, of which the half is for the background collection.

2.3 Atomic Force Microscopy

The topography and surface structure of the graphene films were analyzed by means of the instrument NTEGRA (by NT-MDT). These measurements were performed in semi-contact mode with nanometer resolution.

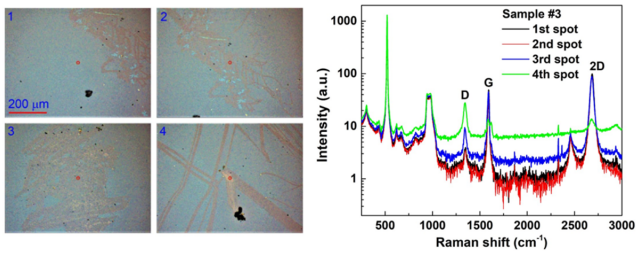

Figure 2: Raman spectra of single layer graphene on Si/SiO_2 taken at 4 different spots corresponding to the optical images on the left where these spots are indicated by small red circles (as guides to the eye). Note the logarithmic scale of the intensity axis of the spectra. The color contrast in optical images in panels $1-4$ suggests scratches. Being possibly superficial, they do not seem to affect the spectra in cases 2 and 3, i.e., the graphene layer is preserved. On the other hand, the spectrum of spot 4 shows that the $2D$ and G graphene peaks are much lower than the D peak, suggesting that the graphene layer does not survive the scratch. Possibly deeper scratch also is suggested by somehow different color at the location of spot 4.

3 RESULTS AND DISCUSSION

The results in Fig. 1 above refer to pristine graphene samples. Let us now compare them with the ones after our treatment in $n-$heptane. One of the most interesting cases is shown in Fig. 2.

During the $n-$heptane treatment, certain scratches have been introduced (commented in figure caption), which assist in understanding the overall situation, as will be explained now. For spots $1-3$, the $G-$peak is twice smaller than the $2D-$peak (taking into account the log-scale of the plots in Fig. 2). This means that the scratches in case of spots 2 and 3 are on top of the graphene layer. That is, there is a scratchable layer everywhere on the sample, and that this layer is undetectable by the Raman diagnostics (since the data for spot 1 are similar to those for spots 2 and 3). For a deeper scratch, such as in spot 4, graphene is indeed removed, as Fig. 2 documents. The occurrence of this most likely organic layer is related to the graphene transfer procedures, as we mentioned in the Introduction. Researchers associate the incomplete removal of organic remnants with insolubility in acetone or other liquids used for this task. These results provide unequivocal evidence about insufficiency of plain Raman spectroscopy for characterization of functional readiness of the graphene surface for electronic applications, including our ideal diamagnetism studies. Interestingly, $n-$heptane treatment, as we will see below, visualizes it without any mechanical scratching and assists in the removal of these residues. Figure 3 illustrates this statement.

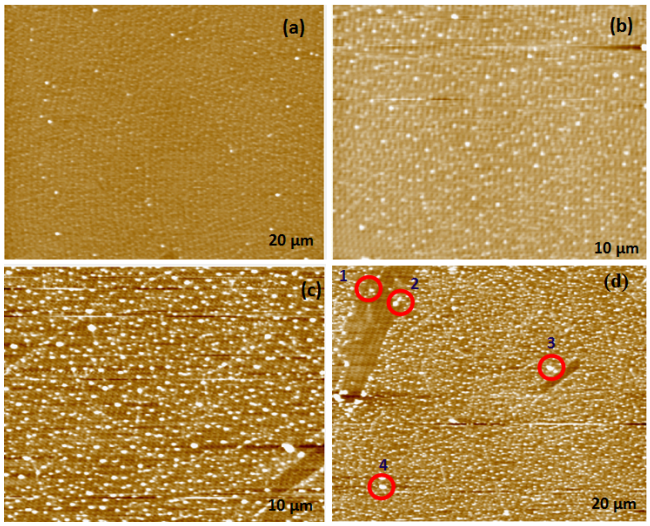

Figure 3: AFM images of single-layer graphene on Si/SiO_2 substrate: (a) before immersing into $n-$heptane; (b) annealed at 200°C for 2 h prior to soaking into $n-$heptane for 1/2 h; (c) soaked in $n-$heptane once for 1/2 h; (d) soaked twice (for 1/2 h each) and annealed at 200°C for 2 h. The outlined areas in (c) correspond to "nanomountains" characterized by surface topography (see Table 1).

Table 1: Typical "nanomountain" heights

Zones	1	2	3	4
Height (nm)	6	9	12	30

The most drastic feature visible from Fig. 3 is the appearance of precipitation of localized nano-scale objects. These objects have heights from units to tens of nanometers, as follows from Table 1; we called them "nanomountains"

Very interestingly, "nanomountains" appear after vacuum annealing of pristine (unused) graphene where they were being initially absent (Fig. 4, panels *a* and *b*).

Most likely, this is due to the residues left after the graphene transfer between it and the substrate. Figure 4 also demonstrates a clear shift in the Raman spectrum of graphene after vacuum annealing. Both G and 2D peaks are shifted, only G is shown. These initial results have been further explored, and a more detailed description will be presented elsewhere.

4 CONCLUSION

Complementary usage of Raman and AFM techniques allowed us to reveal properties of pristine and used in experiments graphene layers which have crucial importance regarding reproducibility in variety of applications in microelectronics.

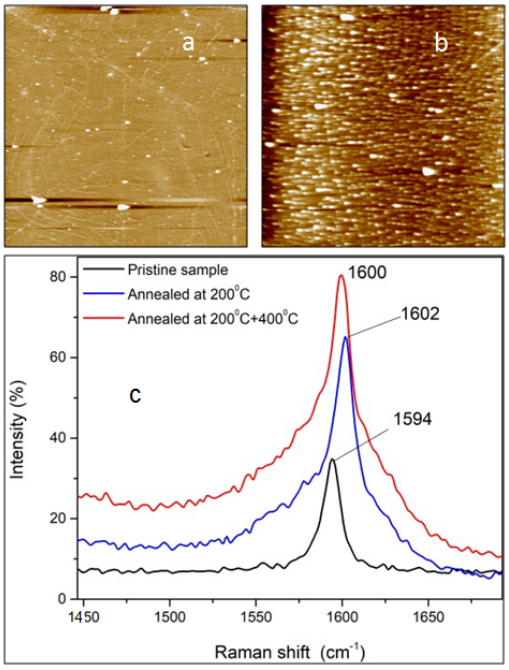

Figure 4: After annealing of pristine graphene where the nanomountains were initially absent (a) they appear at high-vacuum annealing at 200°C (b). Also there is a Raman shift related to this annealing; the G-peak shift is shown in (c).

In addition to wrinkle and cluster-type domains, the graphene films transferred from the original CVD-grown copper supports frequently have remnant organic residues both on the top and the bottom of the pristine graphene. These layers may not be visible by usual Raman diagnostics, and consequently "good" graphene samples may fail in reproducing expected electronic properties. High-vacuum thermal treatment may reveal the hidden residues, though this process can result in unwanted shift in phonon properties of the graphene, which, in turn, may have its own influence on the electronic features. Further research is required for achieving reproducibility of graphene-based electronic devices.

ACKNOWLEDGMENTS

We would like to express gratitude to Y. Kawashima, X. Liang and C.A. Richter for useful discussions. This research was supported in part by the ONR grants N00014-18-1-2636, N00014-19-1-2265, and N00014-20-1-2442.

REFERENCES

[1] C. Backes, A. M. Abdelkader, C. Alonso, *et al.*, *2D Materials*, vol. 7, no. 2, p. 022001, 2020.

[2] P. Mustonen, D. M. A. Mackenzie, and H. Lipsanen, *Frontiers of Optoelectronics*, vol. 13, no. 2, pp. 91–113, 2020.

[3] F. Larki, Y. Abdi, P. Kameli, and H. Salamati, *Photonic Sensors*, 2020.
[4] A. B. Suriani, Muqoyyanah, A. Mohamed, S. Alfarisa, M. H. Mamat, M. K. Ahmad, M. D. Birowosuto, and T. Soga, *Bulletin of Materials Science*, vol. 43, no. 1, p. 310, 2020.
[5] J. Shan, J. Sun, and Z. Liu, *ChemNanoMat*, vol. 7, no. 5, pp. 515–525, 2021.
[6] Y. Xu and J. Liu, *Small*, vol. 12, no. 11, pp. 1400–1419, 2016.
[7] N. Villa, J. D. Zapata, and D. Ramirez, *Thin Solid Films*, vol. 721, p. 138556, 2021.
[8] Z. Wu, X. Zhang, A. Das, J. Liu, Z. Zou, Z. Zhang, Y. Xia, P. Zhao, and H. Wang, *RSC Adv.*, vol. 9, pp. 41 447–41 452, 2019.
[9] B. H. Son and Y. H. Ahn, *Journal of the Korean Physical Society*, vol. 75, no. 10, pp. 817–820, 2019.
[10] B. Zhuang, S. Li, S. Li, and J. Yin, *Carbon*, vol. 173, pp. 609–636, 2021.
[11] X. Liang, B. A. Sperling, I. Calizo, G. Cheng, C. A. Hacker, Q. Zhang, Y. Obeng, K. Yan, H. Peng, Q. Li, X. Zhu, H. Yuan, A. R. Hight Walker, Z. Liu, L.-m. Peng, and C. A. Richter, *ACS Nano*, vol. 5, no. 11, pp. 9144–9153, 2011.
[12] Y.-H. Deng, *arXiv*, vol. 2010.11534, 2020.
[13] X. Li, Y. Zhu, W. Cai, M. Borysiak, B. Han, D. Chen, R. D. Piner, L. Colombo, and R. S. Ruoff, *Nano Letters*, vol. 9, no. 12, pp. 4359–4363, 2009.
[14] K. Shahzad, K. Jia, C. Zhao, X. Yan, Z. Yadong, M. Usman, and J. Luo, *Nanoscale Research Letters*, vol. 15, no. 1, p. 85, 2020.
[15] Y.-C. Lin, C.-C. Lu, C.-H. Yeh, C. Jin, K. Suenaga, and P.-W. Chiu, *Nano Letters*, vol. 12, no. 1, pp. 414–419, 2012.
[16] E. A. Kolesov, M. S. Tivanov, O. V. Korolik, E. Y. Kataev, F. Xiao, O. O. Kapitanova, H. D. Cho, T. W. Kang, and G. N. Panin, *Journal of Physics D: Applied Physics*, vol. 53, no. 4, p. 045302, 2019.
[17] L. Sun, L. Lin, Z. Wang, D. Rui, Z. Yu, J. Zhang, Y. Li, X. Liu, K. Jia, K. Wang, L. Zheng, B. Deng, T. Ma, N. Kang, H. Xu, K. S. Novoselov, H. Peng, and Z. Liu, *Advanced Materials*, vol. 31, no. 43, p. 1902978, 2019.
[18] A. M. Goossens, V. E. Calado, A. Barreiro, K. Watanabe, T. Taniguchi, and L. M. K. Vandersypen, *Applied Physics Letters*, vol. 100, no. 7, p. 073110, 2012.
[19] Y. Lee, S. Bae, H. Jang, S. Jang, S.-E. Zhu, S. H. Sim, Y. I. Song, B. H. Hong, and J.-H. Ahn, *Nano Letters*, vol. 10, no. 2, pp. 490–493, 2010.
[20] J. Shim, C. H. Lui, T. Y. Ko, Y.-J. Yu, P. Kim, T. F. Heinz, and S. Ryu, *Nano Letters*, vol. 12, no. 2, pp. 648–654, 2012.
[21] J. Li, S. Wieghold, M. A. Öner, P. Simon, M. V. Hauf, E. Margapoti, J. A. Garrido, F. Esch, C.-A. Palma, and J. V. Barth, *Nano Letters*, vol. 14, no. 8, pp. 4486–4492, 2014.
[22] B. Li, K. Tahara, J. Adisoejoso, W. Vanderlinden, K. S. Mali, S. De Gendt, Y. Tobe, and S. De Feyter, *ACS Nano*, vol. 7, no. 12, pp. 10 764–10 772, 2013.
[23] A. C. Ferrari and D. M. Basko, *Nature Nanotechnology*, vol. 8, no. 4, pp. 235–246, 2013.
[24] Y. Kawashima, R. Dulal, S. Teknowijoyo, S. Chahid, and A. Gulian, *Modern Physics Letters B*, vol. 34, no. 36, p. 2050415, 2020.
[25] T. Yang, S. Berber, J.-F. Liu, G. P. Miller, and D. Tománek, *The Journal of Chemical Physics*, vol. 128, no. 12, p. 124709, 2008.
[26] C. Chauveau, M. Birouk, F. Halter, and I. Gökalp, *International Journal of Heat and Mass Transfer*, vol. 128, pp. 885–891, 2019.
[27] Y. Huang, J. Lu, and S. Meng, *2D Materials*, vol. 5, no. 4, p. 041001, 2018.
[28] F. Jiménez-Ángeles, K. J. Harmon, T. D. Nguyen, P. Fenter, and M. Olvera de la Cruz, *Phys. Rev. Research*, vol. 2, p. 043244, 2020.
[29] S. Burikov, T. Dolenko, S. Patsaeva, Y. Starokurov, and V. Yuzhakov, *Molecular Physics*, vol. 108, no. 18, pp. 2427–2436, 2010.
[30] L. Kong, A. Enders, T. S. Rahman, and P. A. Dowben, *Journal of Physics: Condensed Matter*, vol. 26, no. 44, p. 443001, 2014.
[31] J. S. Bunch, S. S. Verbridge, J. S. Alden, A. M. van der Zande, J. M. Parpia, H. G. Craighead, and P. L. McEuen, *Nano Letters*, vol. 8, no. 8, pp. 2458–2462, 2008.
[32] S. A. Svatek, O. R. Scott, J. P. Rivett, K. Wright, M. Baldoni, E. Bichoutskaia, T. Taniguchi, K. Watanabe, A. J. Marsden, N. R. Wilson, and P. H. Beton, *Nano Letters*, vol. 15, no. 1, pp. 159–164, 2015.